J. Cent. South Univ. (2016) 23: 2558−2569
DOI: 10.1007/s11771-016-3317-4

Springer

Load-induced error identification of hydrostatic turntable and its influence on machining accuracy

CHENG Qiang(程强), REN Wei-da(任伟达), LIU Zhi-feng(刘志峰), CHEN Dong-ju(陈东菊), GU Pei-hua(顾佩华)

College of Mechanical Engineering and Applied Electronics Technology, Beijing University of Technology, Beijing 100124, China

Abstract: In heavy duty machine tools, hydrostatic turntable is often used as a means for providing rotational motion and supporting workpiece, so the accuracy of turntable is crucial for part machining. In order to analyze the influence of load-indcued errors on machining accuracy, an identification model of load-induced errors based on the deformation caused by applied load of hydrostatic turntable of computerized numerical control (CNC) gantry milling heavy machine is proposed. Based on multi-body system theory and screw theory, the space machining accuracy model of heavy duty machine tool is established with consideration of identified load-induced errors. And then, the influence of load-induced errors on space machining accuracy and the roundness error of a milled hole is analyzed. The analysis results show that load-induced errors have a big influence on the roundness error of machined hole, especially when the center of the milled hole is far from that of hydrostatic turntable.

Key words: machine tool; load-induced error; geometric error; hydrostatic turntable; screw theory

1 Introduction

With the increasing requirements of high metal-removal rate and high productivity [1], multi-axis machine tools are extensively used in manufacturing industry. However, addition of rotary axes is prone to numerous error sources, making the calibration process more difficult [2]. According to results of LEI et al [3], rotary axes are the major error sources in multi-axis machine tools. In heavy duty machine tools, the location of a hydrostatic turntable rotary axis constitutes a significant error source [4]. Therefore, the accuracy of turntable is crucial for part manufacturing with multi-axis machine tools [5]. LIN et al [6] proposed a modified formulation accounting for the corner effect on the flow resistance of the rectangular hydrostatic bearing. CHEN et al [7] used finite element method to study the static and dynamic behavior of a shaft supported by hydrostatic bearings. LIN [8] analyzed the surface roughness, centripetal inertia and recess volume fluid compressibility effects on a hydrostatic bearing. YACOUT et al [9] analyzed the surface roughness and the predominant centripetal inertia terms due to the shaft rotation of the externally pressurized thrust spherical bearings. NADUVINAMANI et al [10] presented a theoretical study on the effects of MHD and surface roughness on the couple stresses squeeze film lubrication between circular stepped plates. HSU et al [11] investigated the performance of ferrofluids to enhance the design of journal bearing within a magnetic field.

Error sources in multi-axis machine tools are due to the flaws in components and joints. MEKID and OGEDENGBE [12] have listed geometric errors, thermally induced errors, and load-induced errors as the three main factors. For geometric errors caused by mechanical imperfections and misalignments are most significant [13], most of the recent research has focused on the reduction or compensation of it [14−15]. Load-induced errors badly affect the stiffness of a machine tool structure for internal or external forces producing unavoidable stresses and strains causing elastic strain with distributed or varying effects [16]. The magnitude of load-induced errors depends on the object loading behaviour, object weight, machining forces, and unbalanced unforeseen forces [17], and a lot of research work on load-induced error compensation has been found to improve machine accuracy [18−19].

To improve the accuracy of hydrostatic turntable machine finally accomplished by error compensation, plenty of research work based on hydrodynamic characteristics of the bearing oil has been found to

Foundation item: Projects(51575010, 51575009) supported by the National Natural Science Foundations of China; Project(Z1511000003150138) supported by Beijing Nova Program, China
Received date: 2015−10−28; **Accepted date:** 2016−03−14
Corresponding author: LIU Zhi-feng, Professor; Tel: +86−10−82317756; E-mail: liuzhifeng187@gmail.com

analyze the whole model of the hydrostatic turntable guideway. SHAMOTO and PARK [20] developed a new model to analyze motion accuracy of hydrostatic feed tables and proposed an algorithm to improve their accuracy. EKINCI and MAYER [21] investigated the relationship between the motion errors of the axis carriage and the guideways' geometric errors both mathematically and experimentally. KHIM and PARK [22] introduced a corrective machining algorithm to improve the motion accuracy of linear motion bearing tables. PARK [23−26] introduced a new method using a transfer function for analyzing the motion errors of hydrostatic bearing tables, which shows good agreement with the motion errors calculated by the Multi Pad Method. ALEYAASIN et al [27] considered a high precision grinding wheel as a rigid rotor mounted on two hydrostatic bearings which proposed an optimization algorithm considering speed.

In view of the present situation, although the research on the hydrodynamic characteristics of hydrostatic bearings and the modeling method of the hydrostatic turntable have been given lots of attention, the research of load-induced error caused by the tilt of the turntable ralated to the hydrodynamic characteristics is still needed. So in this work, in order to analyze the influence of load-indcued errors on the machining accuracy, an identification model of load-induced errors based on the deformation caused by applied load of the hydrostatic turntable is proposed.

2 Load-induced error identification

2.1 Deformation of hydrostatic turntable

A CNC heavy gantry milling machine tool was selected as illustrative example, and its structure frame is shown in Fig. 1. The gantry milling machine can be divided into: countertop (c-axis), lathe bed, apron (y-axis), ram (z-axis). The diameter of the hydrostatic turntable of the heavy gantry milling machine tool is 10 m.

In Fig. 2, a hydrostatic bearing is used as the main shaft bearing of hydrostatic turntable, which makes the

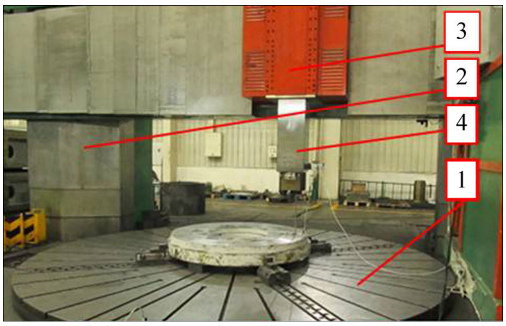

Fig. 1 CNC heavy gantry milling machine tool: 1−Countertop (c-axis); 2−Lathe bed; 3−Apron (y-axis); 4−Ram (z-axis)

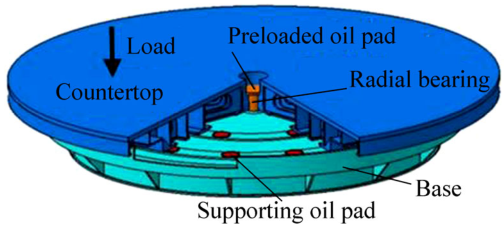

Fig. 2 Structure diagram of hydrostatic turntable

spindle function of the turntable as well as its motor function integrated in the structure. The movement of load is supported by the hydrostatic bearing with the viscous fluid flowing in the small gap between the moving parts and the stationary parts.

In Fig. 3, when the countertop of the turntable is under load, the countertop will be inclined (For example, with the material removing during machining process, the gravity center of the parts might be changed), which will cause deformation at the same time.

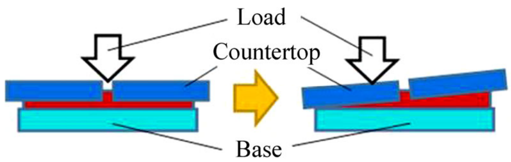

Fig. 3 Sketch map of countertop deformation

As shown in Fig. 4, the hydrostatic turntable of the heavy machine tool is supported by hydrostatic bearing, in which, 24 supporting oil (inside 8, outside 16) pads provide upward support force, and one preloaded oil pad provides downward preload. Ignoring the influence of cutting force on the precision of the machine tool, the influence of the concentrated load force to the deformation of the countertop is analyzed. According to the stress characteristics of the hydrostatic turntable, the force model is simplified to the resultant force of multiple concentration forces.

In Fig. 4, as for the oil within the oil pad, with consideration of its flow characteristics in the machine

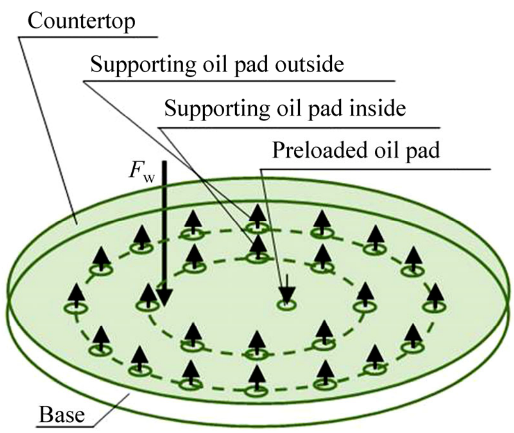

Fig. 4 Force model of hydrostatic turntable

operation process, the oil can be regarded as Newtonian fluid [28]. In this research, it is assumed that the oil fluid can not be compressed and its height is far less than the radius, which makes the oil liquid in the turntable is consistent with the film lubrication theory. So, the N-S equations of the oil pad can be simplified as [29]

$$\frac{1}{r}\cdot\frac{\partial(r\cdot u_r)}{\partial r}+\frac{1}{r}\cdot\frac{\partial(u_\varphi)}{\partial\varphi}+\frac{\partial(u_z)}{\partial z}=0 \tag{1}$$

$$\frac{\partial p}{\partial r}=\eta\cdot\frac{\partial^2 ur}{\partial z^2}+\rho\cdot\frac{u_\varphi{}^2}{r} \tag{2}$$

$$0=\eta\cdot\frac{\partial^2 u_\varphi}{\partial z^2} \tag{3}$$

$$\frac{\partial p}{\partial r}=0 \tag{4}$$

Considering the boundary conditions above, the Reynolds equation is obtained as

$$\frac{1}{r}\cdot\frac{\partial}{\partial r}\left(\frac{rh^3}{12\eta}\frac{\partial p}{\partial r}\right)=\frac{\partial h}{\partial t} \tag{5}$$

The structure diagram of supporting oil pad is shown in Fig. 5.

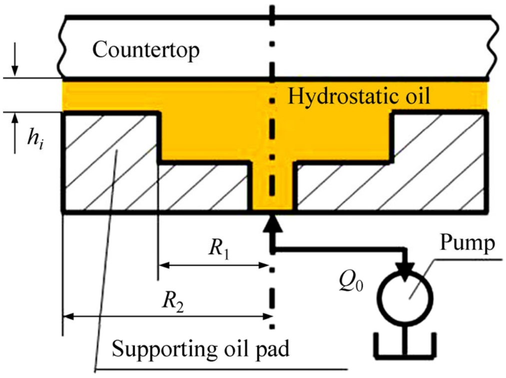

Fig. 5 Structure diagram of supporting oil pad

Integrating Eq. (5) by boundary conditions $r=R_1$, $p=p_0$; $r=R_2$, $p=0$, the bearing pressure of a single supporting oil pad can be gotten with Reynolds equation.

$$F=\pi R_i{}^2 p_0+2\pi\int_{R_1}^{R_2} rp(\mathrm{r})\,\mathrm{d}r=\frac{3\eta Q_0(R_2^2-R_1^2)}{h_i^3}-\frac{3\pi\rho V_\alpha^2(R_2^2-R_1^2)}{40}+\frac{3\pi\eta(R_2^4-R_1^4)\frac{\partial h_i}{\partial t}}{2h2} \tag{6}$$

where V_α is the rotating speed of the hydrostatic turntable; Q_0 is the oil supply for supporting oil pad, which is defined by designers.

The structure diagram of preloaded oil pad is shown in Fig. 6.

As shown in Fig. 6, the boundary conditions are: $z=h$, $u_r=0$, $V_z=\partial h/\partial t$; $z=0$, $u_r=0$, $V_z=0$, then the Reynolds

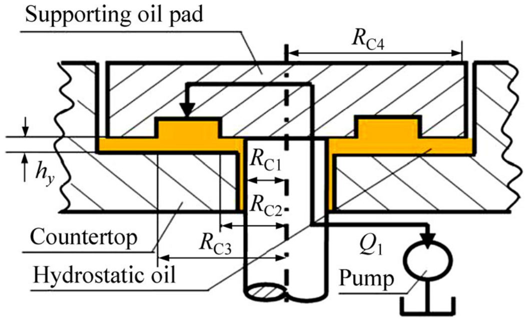

Fig. 6 Structure diagram of preloaded oil pad

equation is obtained as

$$\frac{1}{r}\cdot\frac{\partial}{\partial r}\left(\frac{rh^3}{12\eta}\frac{\partial p}{\partial r}-\frac{\rho\Omega^2 r^2 h^3}{40\eta}\right)=\frac{\partial h}{\partial t} \tag{7}$$

Considering of the action of boundary oil, the bearing pressure of preloaded oil pad can be described:

$$\begin{aligned}F_y&=\pi(R_{C3}^2-R_{C2}^2)p_{0y}+2\pi\int_{R_{C1}}^{R_{C2}} rp_{1y}(r)\mathrm{d}r+2\pi\int_{R_{C4}}^{R_{C3}} rp_{2y}(r)\mathrm{d}r\\&=\frac{3\eta}{2h_y^3\ln\left(\frac{R_{C1}R_{C3}}{R_{C2}R_{C4}}\right)}\left[2Q_1\left((R_{C4}^2-R_{C3}^2)\ln\left(\frac{R_{C1}}{R_{C2}}\right)+(R_{C1}^2-R_{C2}^2)\ln\left(\frac{R_{C3}}{R_{C4}}\right)\right)+\pi\left((R_{C1}^4-R_{C2}^4+R_{C3}^4-R_{C4}^4)\cdot\ln\left(\frac{R_{C1}R_{C3}}{R_{C2}R_{C4}}\right)-\left(R_{C1}^2-R_{C2}^2+R_{C3}^2-R_{C4}^2\right)^2\right)\cdot\frac{\partial h_y}{\partial t}\right]-\\&\frac{3\pi\rho\Omega^2\left(R_{C1}^2-R_{C2}^2+R_{C3}^2-R_{C4}^2\right)}{40\ln\left(\frac{R_{C1}R_{C3}}{R_{C2}R_{C4}}\right)}\left(\left(R_{C1}^2+R_{C2}^2+R_{C3}^2-R_{C4}\right)\ln\left(\frac{R_{C1}}{R_{C2}}\right)-(-R_{C1}^2+R_{C2}^2+R_{C3}^2+R_{C4}^2)\ln\left(\frac{R_{C3}}{R_{C4}}\right)+\left(R_{C1}^2-R_{C2}^2+R_{C3}^2-R_{C4}^2\right)\right)\end{aligned} \tag{8}$$

where Q_1 is the oil supply for preloaded oil pad, which can be calculated by Eq. (8) and Eq. (9) while the turntable is in initial equilibrium state: $h=h_0$, $\theta_x=0$, $\theta_y=0$.

From above equations, the mechanical equilibrium schematic diagram of the countertop is shown in Fig. 7.

As shown in Fig. 7, the turntable is supported by two laps of oil pads, consisting of 24 oil pads. For the supporting oil pads inside, their supporting forces are F_i (i=1−8); the angles between lines connecting oil pads and loading point as well as lines connecting oil pads and the center of countertop are $\varphi_i=2\pi(i-1)/8$ (i=1−8). the distance between center of oil pads center and center of turntable is R_L. For the supporting oil pads outside,

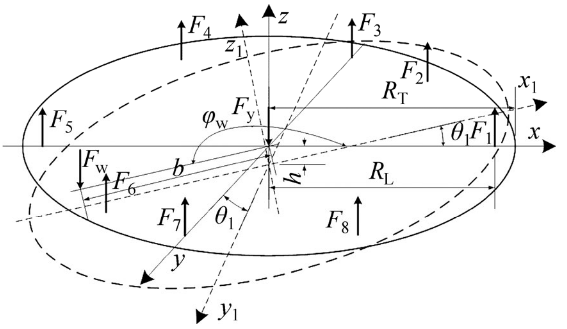

Fig. 7 Force structure diagram of countertop

their supporting forces are F_j (j=1−16); the angles between lines connecting oil pads and loading point as well as lines connecting oil pads and the center of the countertop are φ_j=2π(j−0.5)/16 (j=1−16); the distance between center of oil pads center and center of turntable is R_S. The pre-tightening force of preloaded oil pads is F_y. The radius of turntable is R_T. The rotating speed of turntable is w. The load is F_w, and the angle between x-axis and the line connecting loading point and center of turntable is φ_w; the distance between loading point and center of turntable is R_w. The average value of oil film thickness of all supporting oil pads is h, which equals the sum of the displacement of the center of turntable in vertical direction (Δh_z) and the initial thickness of oil film (h_0). The tilt angles of x-axis and y-axis of turntable are respectively θ_x and θ_y. Obviously, the maximum tilt angle of the turntable is θ_0, θ_0= arctan(R_L/h_0). Assuming no deformation in the turntable, the dynamic equilibrium equation of the turntable can be obtained.

$$\begin{cases} \sum_{i=1}^{8} F_i + \sum_{j=1}^{16} F_j - F_y - F_w - Mg = M\dfrac{\mathrm{d}^2 h}{\mathrm{d}t^2} \\ \sum_{i=1}^{8} F_i R_L \sin\varphi_i + \sum_{j=1}^{16} F_j R_S \sin\varphi_j - F_w R_w \sin(\varphi_w + wt) = \\ \quad J\dfrac{\mathrm{d}^2\theta_x}{\mathrm{d}t^2} \\ \sum_{i=1}^{8} F_i R_L \cos\varphi_i + \sum_{j=1}^{16} F_j R_S \cos\varphi_j - F_w R_w \cos(\varphi_w + wt) = \\ \quad J\dfrac{\mathrm{d}^2\theta_y}{\mathrm{d}t^2} \end{cases} \tag{9}$$

In Eq. (9), M is the quality of the turntable; J is the rotating inertia of the turntable under the action of eccentric force F_w and can be calculated as $J=\dfrac{1}{4}MR_T^2$.

In this work, only steady state problem is considered, and the differential item about time t can be neglected above all, so each equation can be changed to:

$$F_i = \frac{3\eta Q_0({R_2}^2 - {R_1}^2)}{h_i^3} - \frac{3\pi\partial {V_\alpha}^2({R_2}^2 - {R_1}^2)}{40\eta} \tag{10}$$

$$\varphi_i = 2\pi(i-1)/8 \quad (i = 1-8) \tag{11}$$

$$F_j = \frac{3\eta Q_0(R_2^2 - R_1^2)}{h_j^3} - \frac{3\pi\partial V_\alpha^2(R_2^2 - R_1^2)}{40\eta} \tag{12}$$

$$\varphi_j = 2\pi(j-0.5)/16 \quad (j = 1-16) \tag{13}$$

$$F_y = \frac{3\eta}{2h_y^3 \ln\left(\dfrac{R_{C1}R_{C3}}{R_{C2}R_{C4}}\right)}\left[2Q_1\left(\left(R_{C4}^2 - R_{C3}^2\right)\ln\left(\frac{R_{C1}}{R_{C2}}\right) + \left(R_{C1}^2 - R_{C2}^2\right)\ln\left(\frac{R_{C3}}{R_{C4}}\right)\right) - [3\pi\rho w(R_{C1}^2 - R_{C2}^2 + R_{C3}^2 - R_{C4}^2)]/[40\ln\left(\frac{R_{C1}R_{C3}}{R_{C2}R_{C4}}\right)\right] \left((R_{C1}^2 + R_{C2}^2 + R_{C3}^2 - R_{C4}^2)\ln\left(\frac{R_{C1}}{R_{C2}}\right) - (-R_{C1}^2 + R_{C2}^2 + R_{C3}^2 + R_{C4}^2)\ln\left(\frac{R_{C3}}{R_{C4}}\right) + (R_{C1}^2 - R_{C2}^2 + R_{C3}^2 - R_{C4}^2)\right) \tag{14}$$

$$\begin{cases} \sum_{i=1}^{8} F_i + \sum_{j=1}^{16} F_j - F_y - F_w - Mg = 0 \\ \sum_{i=1}^{8} F_i R_L \sin\varphi_i + \sum_{j=1}^{16} F_j R_S \sin\varphi_j - \\ \quad F_w R_w \sin(\varphi_w + wt) = 0 \\ \sum_{i=1}^{8} F_i R_L \cos\varphi_i + \sum_{j=1}^{16} F_j R_S \cos\varphi_j - \\ \quad F_w R_w \cos(\varphi_w + wt) = 0 \end{cases} \tag{15}$$

$$\begin{cases} h_i = h + R_L \sin\varphi_i \tan\theta_x + R_L \cos\varphi_i \tan\theta_y \\ h_j = h + R_S \sin\varphi_j \tan\theta_x + R_S \cos\varphi_j \tan\theta_y \\ h_y = h_{y0} + h_0 + h \end{cases} \tag{16}$$

Among those equations, i=1−8, j=1−16.

Solving Eq. (10) to Eq. (16) by Gauss-Newton method and MATLAB [30], the numerical solution of the countertop deformation (h, θ_x, θ_y) can be obtained.

2.2 Load-induced error identification of turntable

In Section 2.1, the countertop deformation caused by eccentric load of hydrostatic turntable is obtained. It influences positioning accuracy of turntable during rotation and leads to machining error, which is expressed as the load-induced error of turntable. This section will focus on the method to convert the countertop deformation to the load-induced error of turntable.

In order to avoid confusion with traditional geometric error, it needs to point out that the geometric errors here are including load-induced errors of turntable. Considering the geometric errors of turntable caused in geometric error produced during the production or assembly process, the method to convert load-induced error of countertop to integrated geometric error of turntable is needed. Based on multi-body system theory [31−32], the topological structure of hydrostatic turntable is established, as shown in Fig. 8.

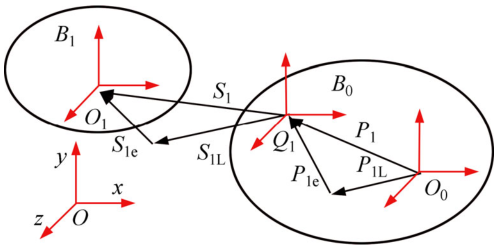

Fig. 8 Topological structure of hydrostatic turntable

According to the structure of turntable and the movement relationship between those parts, the transformation characteristic matrix of each adjacent body is established [33]. Because static errors of moving parts and motion errors of the non-moving parts are relatively small, their error matrices are definited as the unit matrix ($I_{4\times4}$). To facilitate the derivation of back order, the feature matrix of turntable components T is shown in Table 1.

Table 1 Feature matrix of turntable components

Adjacent body	Ideal stationary, motion feature matrix	Stationary, motion feature error matrix
0−1	T_{01p}	ΔT_{01p}
c-axis	ΔT_{01s}	ΔT_{01s}, ΔT_{01F}

In Table 1, p stands for stationary and s stands for motion; $\Delta\alpha$, $\Delta\beta$, $\Delta\gamma$ are angle errors respectively around x-axis, y-axis, z-axis; Δx, Δy, Δz are linear errors along the x-axis, y-axis, z-axis. Each feature matrix is as follows:

$$\Delta \boldsymbol{T}_{01p}=\boldsymbol{I}_{4\times4},\boldsymbol{T}_{01p}=\boldsymbol{I}_{4\times4},\boldsymbol{T}_{01s}=\begin{pmatrix}\cos C & -\sin C & 0 & 0\\ \sin C & \cos C & 0 & 0\\ 0 & 0 & 1 & 0\\ 0 & 0 & 0 & 1\end{pmatrix}$$

$$\Delta \boldsymbol{T}_{01s}=\begin{pmatrix}1 & -\Delta\gamma_C & \Delta\beta_C & \Delta x_C\\ \Delta\gamma_C & 1 & -\Delta\alpha_C & \Delta y_C\\ -\Delta\beta_C & \Delta\alpha_C & 1 & \Delta z_C\\ 0 & 0 & 0 & 1\end{pmatrix}$$

$$\Delta \boldsymbol{T}_{01F}=\begin{pmatrix}1 & -\Delta\gamma_F & \Delta\beta_F & \Delta x_F\\ \Delta\gamma_F & 1 & -\Delta\alpha_F & \Delta y_F\\ -\Delta\beta_F & \Delta\alpha_F & 1 & \Delta z_F\\ 0 & 0 & 0 & 1\end{pmatrix} \tag{17}$$

Tables 2 and 3 show the geometric errors and load-induced errors and their meanings of the turntable.

Table 2 Six motion geometric errors of c-axis

Geometric implication of error	Symbol
c-axial x direction linear error	Δx_c
c-axial y direction linear error	Δy_c
c-axial z direction linear error	Δz_c
Angle error of c-axis around x-axis	$\Delta\alpha_c$
Angle error of c-axis around y-axis	$\Delta\beta_c$
Angle error of c-axis around z-axis	$\Delta\gamma_c$

Table 3 Six load-induced errors of c-axis

Geometric implication of error	Symbol
c-axial x direction linear load-induced error	Δx_F
c-axial y direction linear load-induced error	Δy_F
c-axial z direction linear load-induced error	Δz_F
Angle load-induced error of c-axis around x-axis	$\Delta\alpha_F$
Angle load-induced error of c-axis around y-axis	$\Delta\beta_F$
Angle load-induced error of c-axis around z-axis	$\Delta\gamma_F$

As the numerical solution of the countertop deformation had been obtained in Section 2.1, the load-induced errors of the countertop can be calculated.

Displacement along z-axis of countertop, Δz_F, is

$$\Delta z_F=h-h_0 \tag{18}$$

Tilt angle of x-axis of countertop, $\Delta\alpha_F$, is

$$\Delta\alpha_F=\theta_x \tag{19}$$

Tilt angle of y-axis of countertop, $\Delta\rho_F$, is

$$\Delta\beta_F=\theta_y \tag{20}$$

Because the mechanical equilibrium equation is based on mass center of countertop, defining the countertop height (h_z), h_z=500 mm, the other load-induced errors can be obtained.

Displacement along x-axis of countertop, Δx_F, is

$$\Delta x_F=\frac{1}{2}h_z\sin\theta_x \tag{21}$$

Displacement along y-axis of countertop, Δy_F, is

$$\Delta y_F=\frac{1}{2}h_z\sin\theta_y \tag{22}$$

Because hydrostatic turntable rotates around z-axis, tilt angle of z-axis of countertop, $\Delta\gamma_F$, is

$$\Delta\gamma_F=0 \tag{23}$$

By Eq. (10) to Eq. (16) , the load-induced errors of turntable should be interrelated with the rotating speed of turntable (w), the distance between loading point and center of turntable (R_w), and the loading force (F_w), as well as the angle between x-axis and the line connecting loading point and center of turntable(φ_w).

By Gauss-Newton method and MATLAB, substituting different rotating speed (w), loading force (F_w), and load radius (R_w) into Eq. (15), the numerical solution of load-induced errors can be obtained. Figure 8 shows the different load-induced errors of countertop with different rotation speed.

As shown in Fig. 9, as the rotation speed of w increases gradually, the errors of $\Delta\beta_F$, Δy_F, Δz_F show increasing trend, and $\Delta\alpha_F$, Δx_F show reducing trend, among which $\Delta\beta_F$, Δy_F have the biggest changing amount. The results show that the rotation speed has an influence on load-induced errors of countertop, and the impact range is about a few microns.

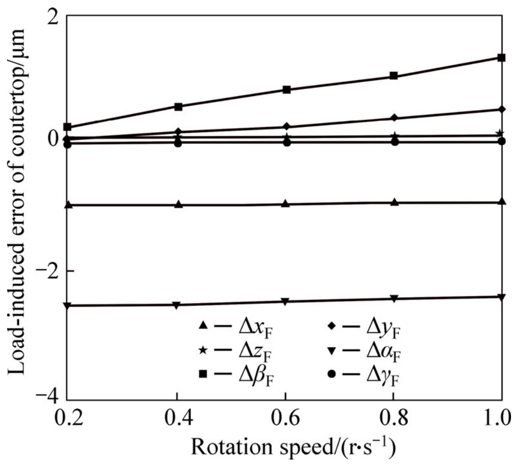

Fig. 9 Countertop load-induced errors with different rotation speed

Figure 10 shows the different load-induced errors of countertop with different loading force. It can be seen that, as the loading force of F_w increases gradually, the errors of Δx_F, Δy_F, Δz_F, $\Delta\alpha_F$, $\Delta\beta_F$ all show increasing trend, among which $\Delta\alpha_F$, Δx_F, $\Delta\beta_F$ have the biggest increasing amount. The results show that, the loading force has

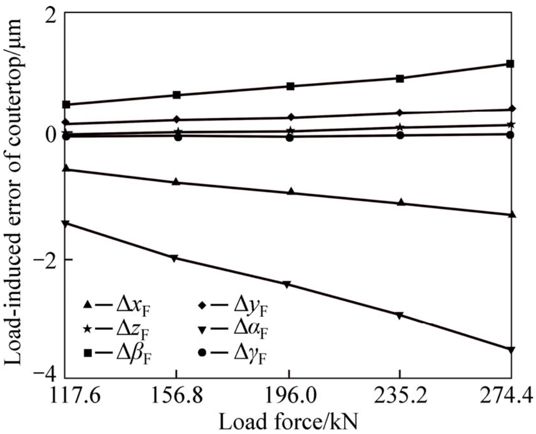

Fig. 10 Countertop load-induced errors with different loading force

an influence on load-induced errors of countertop, which makes all errors increased, and the impact range is about a few microns.

Figure 11 shows the different load-induced errors of countertop with different load radius. It can be seen that, as the load radius of R_w increases gradually, the errors of Δx_F, Δy_F, Δz_F, $\Delta\alpha_F$, $\Delta\beta_F$ all show increasing trend, among which $\Delta\alpha_F$, Δx_F, $\Delta\beta_F$ have the biggest increasing amount. The results show that, the load radius has an influence on load-induced errors of countertop, which makes all errors increase, and the impact range is about a few microns. The influence of load radius on countertop load-induced errors is more obvious than the influence of the loading force.

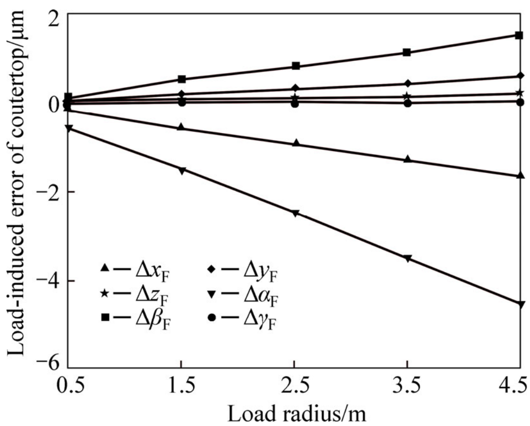

Fig. 11 Countertop load-induced errors with different load radiuses

In machining, the machining accuracy of machine tool is decided by the relative displacement error between tool forming point and workpiece forming point. In the process of establishing the error identification model of turntable, the mathematical relationship between workpiece forming points and workpiece forming points in the condition of the ideal state is demonstrated, which is also the accuracy of the model called $\boldsymbol{E}_{\text{spt}}$:

$$\boldsymbol{E}_{\text{spt}}=\begin{pmatrix}\cos C & -\sin C & 0 & 0\\ \sin C & \cos C & 0 & 0\\ 0 & 0 & 1 & 0\\ 0 & 0 & 0 & 1\end{pmatrix}\cdot \begin{pmatrix}1 & -\Delta\gamma_C & \Delta\beta_C & \Delta x_C\\ \Delta\gamma_C & 1 & -\Delta\alpha_C & \Delta y_C\\ -\Delta\beta_C & \Delta\alpha_C & 1 & \Delta z_C\\ 0 & 0 & 0 & 1\end{pmatrix}\cdot \begin{pmatrix}1 & -\Delta\gamma_F & \Delta\beta_F & \Delta x_F\\ \Delta\gamma_F & 1 & -\Delta\alpha_F & \Delta y_F\\ -\Delta\beta_F & \Delta\alpha_F & 1 & \Delta z_F\\ 0 & 0 & 0 & 1\end{pmatrix}\cdot\begin{pmatrix}-p_{wx}\\ p_{wy}\\ p_{wz}\\ 1\end{pmatrix} \tag{24}$$

In Eq. (24), C is the angle of rotation of the c-axis of turntable; p_{wx}, p_{wy} , p_{wz} represent the initial position of the workpiece, respectively.

The first three terms of the numerical solution of the matrix $\boldsymbol{E}_{\mathrm{spt}}$: E_{spt1}, E_{spt2}, E_{spt3} represent the final position of workpiece, respectively. Therefore, the integrated geometric errors of turntable: Δx_{spt}, Δy_{spt}, Δz_{spt} can be calculated. Table 4 shows the integrated geometric errors and their meanings of turntable. The integrated geometric errors of turntable: Δx_{spt}, Δy_{spt}, Δz_{spt} can be calculated by MATLAB.

Table 4 Integrated geometric errors of turntable/mm

Geometric implication of error	Symbol	Unit
x direction linear error of turntable	Δx_{spt}	mm
y direction linear error of turntable	Δy_{spt}	mm
z direction linear error of turntable	Δz_{spt}	mm

Figure 12 shows the different integrated geometric errors of turntable with different rotation speed. It can be seen that, as the rotation speed of w increases gradually, Δx_{spt} tends to increase slightly, Δy_{spt} tends to increase, and Δz_{spt} tends to decrease. The results show that the rotation speed has an influence on integrated geometric errors of turntable, which makes the horizontal error increase as well as the vertical error reduce as it increases, and the impact range is about a few microns.

Figure 13 shows the different integrated geometric errors of turntable with different loading force. It can be seen that, as the loading force of F_w increases gradually, Δx_{spt} tends to increase, Δy_{spt} tends to increase slightly, and Δz_{spt} tends to increase. The results show that the loading force has an influence on integrated geometric errors of turntable, which makes all errors increase, and the impact range is about a few microns.

Figure 14 shows the different integrated geometric errors of the turntable with different load radius. It can be seen that, as the loading force of F_w increases gradually,

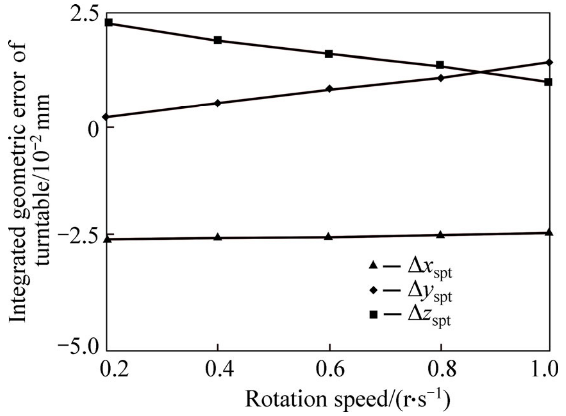

Fig. 12 Turntable integrated geometric errors with different rotation speeds

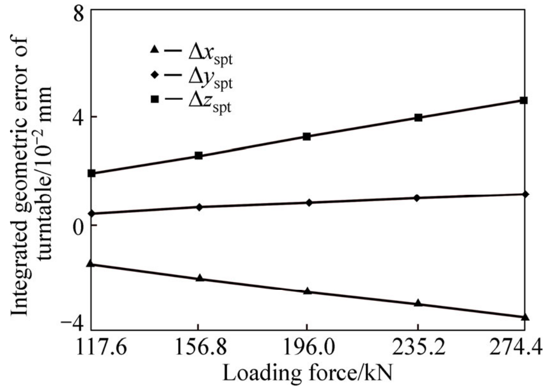

Fig. 13 Turntable integrated geometric errors with different loading forces

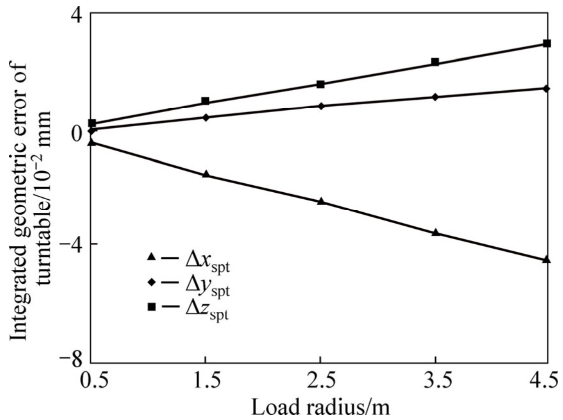

Fig. 14 Turntable integrated geometric errors with different load radius

Δx_{spt} tends to increase, Δy_{spt} tends to increase slightly, and Δz_{spt} tends to increase. The results show that, the load radius has an influence on integrated geometric errors of the turntable, which makes all errors increase, and the impact range is about a few microns. The influence of load radius on turntable integrated geometric errors is more obvious than that of the loading force.

Figure 15 shows the integrated geometric error test of the turntable with different loading force. In Fig. 16, the experimental verification shows that the maximum difference between integrated geometric errors by calculation and actual measurement error is 0.0081 mm, which meets the modeling requirements basically.

3 Modeling of spatial machining error

3.1 Error model establishment based on topological structure

The integrated geometric errors and their meanings of the illustrative machine tool are listed in Table 5. δ represents linear error, ε represents angular error, and S represents squareness error. P represents parallelism error. δ_{xy} represents the linear error in x-direction when y-axis moves, which means that the first subscript is the

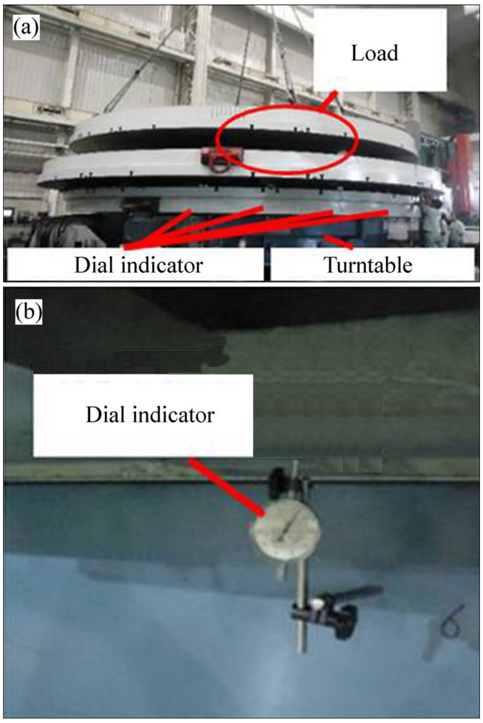

Fig. 15 Integrated geometric error test device of turntable: (a) Test device configuration; (b) Dial indicator

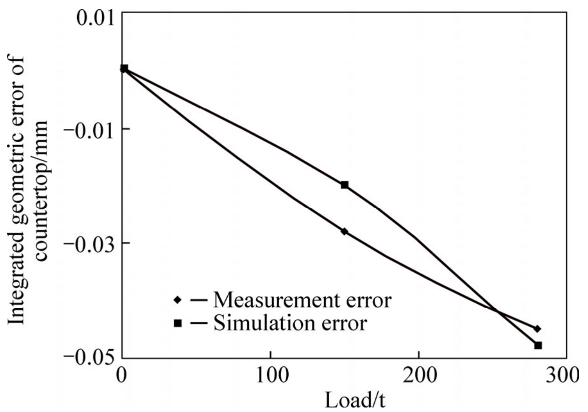

Fig. 16 Experimental verification for integrated geometric error

Table 5 Integrated geometric errors of gantry machine tool

Geometric implication of error	Number of errors	Symbol
Linear positioning error (include z-axis linear load-induced error)	3	δ_{yy}, δ_{zz}, δ_{zC}
Horizontal straightness error (include x-axis linear load-induced error)	3	δ_{zy}, δ_{xz}, δ_{xC}
Vertical straightness error (include y-axis linear load-induced error)	3	δ_{xy}, δ_{yz}, δ_{yC}
Rolling angle error (include z-axis angle load-induced error)	3	ε_{yy}, ε_{zz}, ε_{zC}
Pitch angle error (include x-axis angle load-induced error)	3	ε_{zy}, ε_{xz}, ε_{xC}
Yaw angle error (include y-axis angle load-induced error)	3	ε_{xy}, ε_{yz}, ε_{yC}
Squareness error	2	S_{yz}, S_{yC},
Parallelism error	2	PX_{zC}, PY_{zC},

direction of error and the other is the direction of movement, namely linear axis. As for angular error ε_{xy}, the first subscript is the rotation direction of error and the other is the direction of movement. These geometric errors can be expressed as twists, and the error model can be established using screw theory [34−35].

Based on multi-body system theory [36−37], the movement parts of the machine tool are to set up the corresponding “body” by representation of B_j (j=1, 2, 3, 4). As shown in Fig. 17, the model of the machine tool is arranged in the order of B_j according to the order of c-axis and y-axis to z-axis.

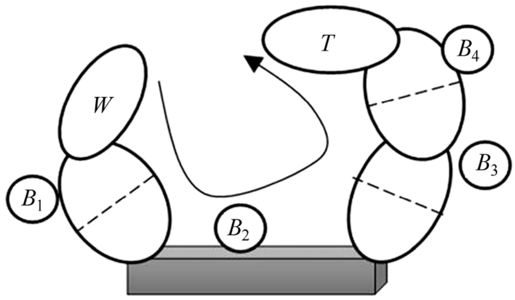

Fig. 17 Machine tool topological structure chart

3.2 Screw model of spatial machining error

In the ideal case, there exist no errors. Then, the order of the model based on the screw theory is shown as $C_i \rightarrow Y_i \rightarrow Z_i$. The ideal transformation matrix, namely the ideal POE model [38], is obtained as $\boldsymbol{T}_i$:

$$\boldsymbol{T}_i = \boldsymbol{e}^{-c\hat{\$}_{C_i}} \cdot \boldsymbol{e}^{-y\hat{\$}_{Y_i}} \cdot \boldsymbol{e}^{-z\hat{\$}_{Z_i}} \tag{25}$$

Considering the error twists, including Parallelism errors, squareness errors, linear errors, and rotation errors, the order of the model is obtained as T_a:

$$\begin{aligned}\boldsymbol{T}_a &= e^{-\hat{\$}_{C_e}} \cdot e^{-c\hat{\$}_{cs}} \cdot e^{\hat{\$}_b} \cdot e^{y\hat{\$}_{ys}} \cdot e^{\hat{\$}_{Y_e}} \cdot e^{z\hat{\$}_{zs}} \cdot e^{\hat{\$}_{Z_e}} = e^{-\hat{\$}_{C_e}} \cdot \\ &\left(e^{-PY_{zC}\hat{\$}_{yr}} \cdot e^{PX_{zC}\hat{\$}_{xr}}\right) \cdot e^{\gamma\hat{\$}_{C_i}} \cdot \left(e^{-PY_{zC}\hat{\$}_{yr}} \cdot e^{PX_{zC}\hat{\$}_{xr}}\right)^{-1} \cdot \\ &e^{\hat{\$}_b} \cdot \left(e^{-S_{yC}\hat{\$}_{yr}}\right) \cdot e^{y\hat{\$}_{Y_i}} \cdot \left(e^{-S_{yC}\hat{\$}_{yr}}\right)^{-1} \cdot e^{\hat{\$}_{Y_e}} \cdot \left(e^{-S_{yz}\hat{\$}_{yr}}\right) \cdot \\ &e^{z\hat{\$}_{Z_i}} \cdot \left(e^{-S_{yz}\hat{\$}_{yr}}\right)^{-1} \cdot e^{\hat{\$}_{Z_e}}\end{aligned} \tag{26}$$

In this equation, $\hat{\$}_b = [0, 0, 0, 0, 0, 0]^{\mathrm{T}}$ represents the machine bed.

The difference between the ideal and the actual homogeneous coordinates of tool tip is the tool tip error. And the error transformation matrix is:

$$\boldsymbol{E} = \boldsymbol{T}_i^{-1} \cdot \boldsymbol{T}_a \tag{27}$$

where $\boldsymbol{E}$ represents the POE model of geometric errors. And the position errors of tool tip in the workpiece coordinate system are E_x, E_y, E_z:

$$\left[E_x, E_y, E_z, 1\right]^{\mathrm{T}} = \boldsymbol{E} \cdot \left[0,0,0,1\right]^{\mathrm{T}} \tag{28}$$

4 Analysis of space machining error

4.1 Space machining error of turntable machine

In Section 3.2, the spatial error model of the heavy gantry hydrostatic turntable machine tool has been obtained. By MATLAB software, the space machining errors represented by E_x, E_y, E_z can be obtained. As known from Section 2.1, the space machining errors of the machine tool should be interrelated with the rotating speed of the turntable(w), the distance between loading point, center of turntable (R_w), and the loading force (F_w), as well as the angle between x-axis and the line connecting loading point and center of turntable (φ_w) .

4.2 Influence of different factors on space machining accuracy

As the screw model known from Section 3.2, with different rotation speed, the space machining errors of the machine tool: E_x, E_y, E_z can be calculated by MATLAB. Table 6 shows different space machining errors of machine tool with different rotation speeds. It can be seen that, as the rotation speed of w increases gradually, E_x tends to decrease, E_y tends to increase, and E_z tends to decrease. The results indicates rotation speed has an influence on space machining accuracy of machine tool, which makes the x-axis error increase, y-axis error reduce and z-axis error reduce as it increases.

Table 6 Space machining errors with different rotation speed

Rotation speed/(r·s^{-1})	Space machining errors/mm		
	E_x	E_y	E_z
0.2	3.2709807×10^{-2}	3.201347213×10^{-2}	3.84×10^{-3}
0.4	3.2709806×10^{-2}	3.201347219×10^{-2}	3.83×10^{-3}
0.6	3.2709805×10^{-2}	3.201347229×10^{-2}	3.81×10^{-3}
0.8	3.2709805×10^{-2}	3.201347242×10^{-2}	3.78×10^{-3}
1.0	3.2709804×10^{-2}	3.201347259×10^{-2}	3.75×10^{-3}

Table 7 shows the different space machining errors of the machine tool with different loading force. It can be seen that, as the loading force of F_w increases gradually, E_x tends to decrease, E_y tends to decrease, E_z tends to increase. The results indicates that loading force has an influence on space machining accuracy of machine tool, which makes the horizontal error reduce as well as the vertical error increase as it increases.

Table 8 shows the different space machining errors of the machine tool with different load radius. It can be seen that, as the load radius of R_w increases gradually, E_x tends to decrease, E_y tends to decrease, E_z tends to increase. The results indicates that load radius has an influence on space machining accuracy of machine tool , which makes the horizontal error reduce as well as the vertical error increase as it increases.

Table 7 space machining error with different loading force

Loading force/kN	Space machining error/mm		
	E_x	E_y	E_z
117.6	3.2709806×10^{-2}	3.201347565×10^{-2}	3.02×10^{-3}
156.8	3.2709806×10^{-2}	3.201347407×10^{-2}	3.42×10^{-3}
196	3.2709805×10^{-2}	3.201347229×10^{-2}	3.81×10^{-3}
235.2	3.2709805×10^{-2}	3.201347032×10^{-2}	4.20×10^{-3}
274.4	3.2709804×10^{-2}	3.201346815×10^{-2}	4.60×10^{-3}

Table 8 Space machining error with different load radius

Load radius/m	Space machining error/mm		
	E_x	E_y	E_z
0.5	3.2709807×10^{-2}	3.201347824×10^{-2}	2.23×10^{-3}
1.5	3.2709806×10^{-2}	3.201347565×10^{-2}	3.02×10^{-3}
2.5	3.2709805×10^{-2}	3.201347229×10^{-2}	3.81×10^{-3}
3.5	3.2709804×10^{-2}	3.201346815×10^{-2}	4.60×10^{-3}
4.5	3.2709802×10^{-2}	3.201346325×10^{-2}	5.38×10^{-3}

5 Roundness error analysis of milling hole

5.1 Factors affecting roundness error

In the process of milling holes in workpieces, the roundness error of a hole is the difference between the maximum and minimum distances from actual processing point to circle center. It can be expreseed as δ_0.

$$\delta_0 = r_{\max} - r_{\min} \tag{29}$$

where $r_{\max}$ and $r_{\min}$ are repestively the maximum and minimum distances between the actual processing point and the circle center.

According to pratical experience, the roundness error of the hole of the workpiece should be related to the distance between the center of the circular hole and the center of the turntable (R), and the radius of the hole (r). To analyze their effect on the hole roundness error, the roundness error of the hole can be obtained by calculating the spatial error model of the heavy gantry hydrostatic turntable machine tool in Section 3.2 by MATLAB.

5.2 Influence of hole radius on roundness error

As shown in Fig. 18, the position of the hole is unchanged (R=0 mm), and the round hole profile changes with different hole radius (r=100−800 mm). The dotted line is the ideal machining curve, and the scattered point line is the actual curve.

It can be drawn from Fig. 19 that the round hole radius error changes with different hole radius. As the hole radius increases gradually, the round hole radius error tends to be unchanged.

As shown in Fig. 20, the round hole roundness error changes with different hole radius. As the hole radius increases gradually, the round hole roundness error tends to increase slightly.

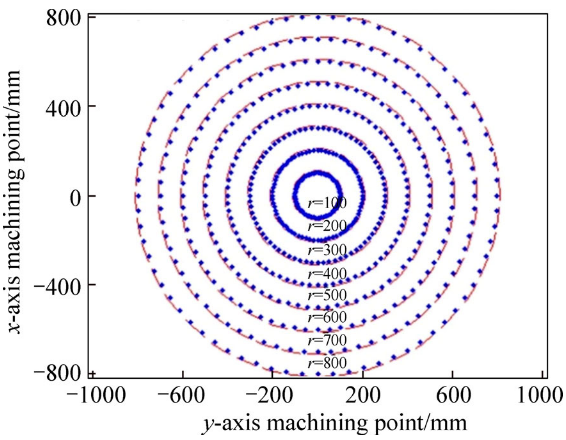

Fig. 18 Changing trend of round hole profile with different hole radiuses

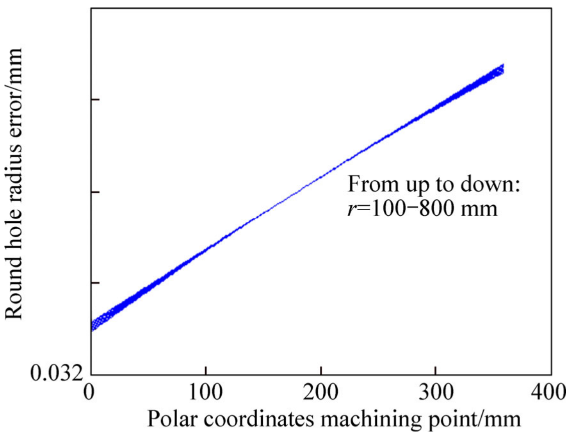

Fig. 19 Changing trend of round hole radius error with different hole radiuses

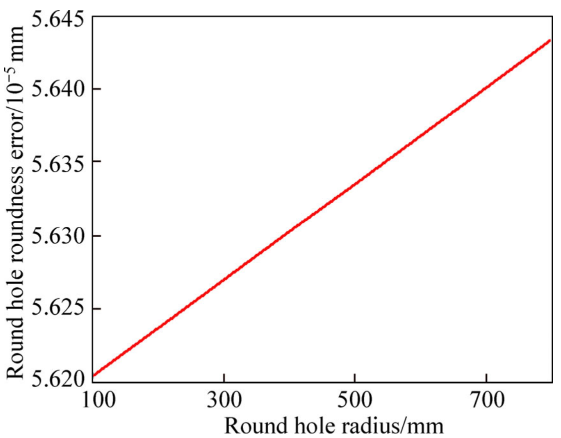

Fig. 20 Changing trend of round hole roundness error with different hole radiuses

5.3 Influence of hole position on roundness error

As shown in Fig. 21, the radius of the hole is unchanged (r=100 mm), and the round hole profile changes with different position of the hole (R=100−800 mm). The dotted line is the ideal machining curve, and the scattered point line is the actual curve.

As shown in Fig. 22, the round hole radius error changes with different positions of the hole. As the distance between the center of the circular hole and the center of the turntable increases gradually, the round hole radius error has large change; however, little fluctuation occurs when only the hole radius changes.

As shown in Fig. 23, the round hole roundness error changes with different position of the hole. As the

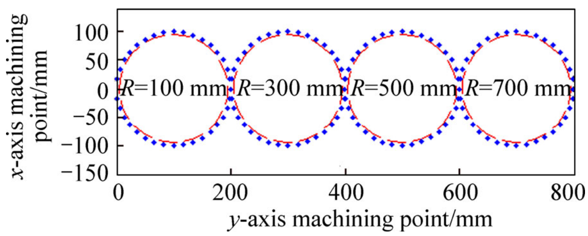

Fig. 21 Changing trend of round hole profile with different hole positions

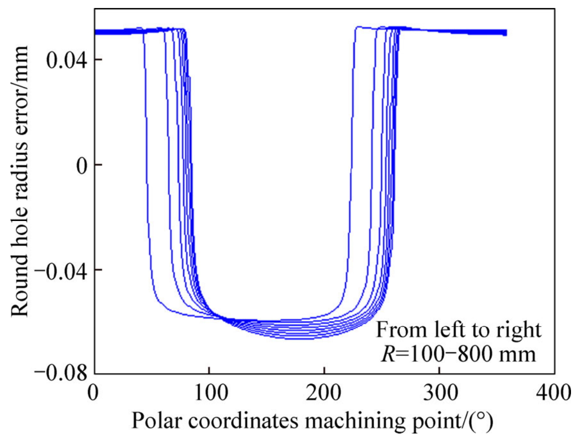

Fig. 22 Changing trend of round hole radius error with different hole positions

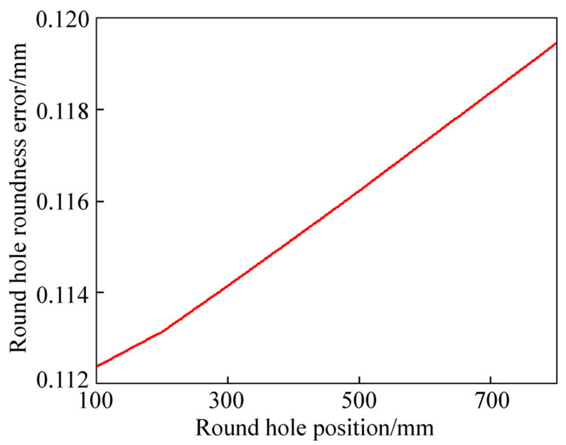

Fig. 23 Changing trend of round hole roundness error with different hole positions

distance between the center of the circular hole and the center of the turntable increases gradually, the round hole roundness error tends to increase.

From above, the results show that, when load-induced errors are considered, with the location of a hole machined fixed, the changes of roundness error of machined hole with different machined hole radius is not obvious. When the radius of the machining hole is unchanged, the change of the roundness error of the machined hole with different machining hole location is more obvious.

6 Conclusions

Geomtric errors, load-induced errors and thermal errors are the main inducments to reduce machining accuracy of heavy duty machine tool. In this work, in order to analyze the influence of load-induced errors on machining accuracy, the deformation caused by applied load of hydrostatic turntable of CNC gantry milling heavy machine is establish based on hydromechanics firstly. And then an identification method of load-induced errors from deformation of turntable is proposed. On the basis of multi-body system theory and screw theory, the space machining accuracy model of heavy duty machine tool is established with consideration of load-induced errors. Finally, the influence of load-induced errors on space machining accuracy and the roundness error of milling a hole is analyzed.

Despite the progress, it should be pointed out that the fuel supply type of turntable analyzed in this work is quantitative type, and turntable using the constant pressure pump is not taken into consideration, which means that the numeriacl solution of the countertop load-induced errors should be calculated differently. Therefore, load-induced errors in different working-conditions need to be further addressed, which is of more practical significance.

Acknowledgement

The authors are most grateful to the Leading Talent Project of Guangdong Province, Open Project of State Key Lab of Digital Manufacturing Equipment & Technology (Huazhong University of Science and Technology), Shantou Light Industry Equipment Research Institute of science and technology Correspondent Station (2013B090900008), China.

References

[1] GAO Xiang-sheng, ZHANG Yi-du, GAO Hao-dong, ZHANG Hong-wei. Dynamic characteristic analysis of whole machine tools based on Kriging model [J]. Journal of Central South University, 2013, 20: 3094− 3102.

[2] RAHMAN M M, MAYER J R R. Five axis machine tool volumetric error prediction through an indirectestimation of intra- and inter-axis error parameters by probing facetson a scale enriched uncalibrated indigenous artefact [J]. Precision Engineering, 2015, 40: 94−105.

[3] LEI W T, PAUNG I M, YU Chen-chi. Total ball bar dynamic tests for five-axis CNC machine tools [J]. Int J Mach Tools Manuf, 2009, 49(6): 488−499.

[4] FLORUSSEN G H J, SPAAN H A M. Dynamic R-test for rotary tables on 5-axes machine tools [J]. Procedia CIRP, 2012, 1: 536−539.

[5] SUH S H, LEE E S, JUNG S Y. Error modelling and measurement for the rotary table of five-axis machine tools [J]. The International Journal of Advanced Manufacturing Technology, 1998, 14(9): 656−663.

[6] LIN Yi-ting, LIAO Chuan-chieh, LIN Ting-yu, LIN Chao-an. Simulations of flow resistances in circular and square hydrostatic bearings [J]. Procedia Engineering, 2014, 79: 114−118.

[7] CHEN Dong-ju, FAN Jin-wei, ZHANG Fei-hu. Dynamic and static characteristics of a hydrostatic spindle for machine tools [J]. Journal of Manufacturing Systems, 2012, 31(1): 26−33.

[8] LIN Jaw-ren. Surface roughness effect on the dynamic stiffness and damping characteristics of compensated hydrostatic thrust bearings [J]. International Journal of Machine Tools and Manufacture, 2000, 40(11): 1671−1689.

[9] YACOUT A W, ISMAEEL A S, KASSAB S Z. The combined effects of the centripetal inertia and the surface roughness on the hydrostatic thrust spherical bearings performance [J]. Tribology International, 2007, 40(3): 522−532.

[10] NADUVINAMANI N B, HANUMAGOWDA B N, TASNEEMFATHIMA S. Combined effects of MHD and surface roughness on couple-stress squeeze film lubrication between porous circular stepped plates [J]. Tribology International, 2012, 56: 19−29.

[11] HSU Tze-chi, CHEN Jing-hong, CHIANG Hsin-lu, CHOU Tsu-liang. Lubrication performance of short journal bearings considering the effects of surface roughness and magnetic field [J]. Tribology International, 2013, 61: 169−175.

[12] MEKID S, OGEDENGBE T I. A review of machine tool accuracy enhancement through error compensation in serial and parallel kinematic machines [J]. Int J Precis Tech, 2010, 1(3): 251−286.

[13] OKAFOR A C, ERTEKIN, YALCIN M. Derivation of machine tool error models and error compensation procedure for three axes vertical machining center using rigid body kinematics [J]. Int J Mach Tool Manu, 2000, 40: 1199−1213.

[14] KHAN A W, CHEN Wu-yi. A methodology for systematic geometric error compensation in five-axis machine tools [J]. Int J Adv Manuf Technol, 2011, 53: 615−628.

[15] FU Guo-qiang, FU Jian-zhong, XU Yue-tong, CHEN Zi-cheng, LAI Jin-tao. Accuracy enhancement of five-axis machine tool based on differential motion matrix: Geometric error modeling, identification and compensation [J]. International Journal of Machine Tools & Manufacture, 2015, 89: 170−181.

[16] KHAN A W, CHEN Wu-yi. Systematic geometric error modeling for workspace volumetric calibration of a 5-axis turbine blade grinding machine [J]. Chinese Journal of Aeronautics, 2010, 23(5): 604−615.

[17] CHENG Qiang, LUO Rui, GU Pei-hua, WANG Zhi-liang, GUO Hong-sheng. Load induced error identification and camber curve design of a large-span crossbeam [J]. Advances in Mechanical Engineering, 2013, 5(5): 847194.

[18] RAKSIRI C, PARNICHKUN M. Geometric and force errors compensation in a 3-axis CNC milling machine [J]. International Journal of Machine Tools and Manufacture, 2004, 44(12/13): 1283−1291.

[19] RATCHEV S, LIU S, HUANG W, BECKER A A. An advanced FEA based force induced error compensation strategy in milling [J]. International Journal of Machine Tools and Manufacture, 2006, 46(5): 542−551.

[20] SHAMOTO E, PARK C H, MORIWAKI T. Analysis and improvement of motion accuracy of hydrostatic feed table [J]. CIRP Annals-Manufacturing Technology, 2001, 50(1): 285−290.

[21] EKINCI T O, MAYER J R R. Investigation of accuracy of erostatic guideways [J]. International Journal of Machine Tools & Manufacture, 2009, 49: 478−487.

[22] KHIM G, PARK C H. Prediction and compensation of motion accuracy in a linear motion bearing table [J]. Precision Engineering, 2011, 35: 393−399.

[23] PARK C H, OH Y J, LEE C H, HONG J H. Theoretical verification on the motion error analysis method of hydrostatic bearing tables using a transfer function [J]. International Journal of the Korean Society of Precision Engineering and Manufacturing, 2003, 4: 64−70.

[24] PARK C H, OH Y J, LEE C H, HONG J H. Experimental verification on a motion error analysis method of hydrostatic bearing tables using a transfer function [J]. International Journal of the Korean Society of Precision Engineering and Manufacturing, 2003, 4: 57−63.

[25] PARK C H, LEE C H, LEE H. Corrective machining algorithm for improving the motion accuracy of hydrostatic bearing tables [J]. International Journal of Precision Engineering and Manufacturing, 2004, 4: 60−67.

[26] PARK C H, LEE C H, LEE H. Experimental verification on the corrective machining algorithm for improving the motion accuracy of hydrostatic bearing tables [J]. International Journal of Precision Engineering and Manufacturing, 2004, 5: 62−68.

[27] ALEYAASIN M, WHALLEY R, EBRAHIMI M. Error correction in hydrostatic spindles by optimal bearing tuning [J]. International Journal of Machine Tools & Manufacture, 2000, 40: 809−822.

[28] CHEN Yan-sheng. The principle and design of hydrostatic bearing [M]. Changsha: National University of Defense Technology Press, 1980: 69−72. (in Chinese)

[29] DONG Xun. Theory of lubrication [M]. Shanglai: Shanghai Jiao Tong University Press, 1984: 80−89. (in Chinese)

[30] LIU Xing-gao, HU Yun-qing. Application of optimization method and matlab implementation [M]. Beijing: Science Press, 2014: 104−108. (in Chinese)

[31] XIONG You-lun. Robotics [M]. Beijing: Press of Machinery Industry, 1993: 24−32. (in Chinese)

[32] FAN Jin-wei. Research on Error Modeling and software compensation of numerical control machine tool based on multi-body system kinematics [J]. Journal of Beijing University of Technology, 1999, 25(2): 39−40. (in Chinese)

[33] CHENG Qiang, LIU Guang-bo, LIU Zhi-feng. A method for identifying key geometric error sources of machine tools based on sensitivity analysis [J]. Journal of Mechanical Engineering, 2012(7): 173−174. (in Chinese)

[34] BAI Shi-xian. Advanced institute [M]. Shanghai: Shanghai Science and Technology Press, 1988: 21−27. (in Chinese)

[35] HUANG Yong-gang, DU Li, HUANG Mao-li. Modeling method of robot error based on the theory of rotation quantity [J]. Journal of Harbin Institute of Technology, 2010, 42(3): 485−486. (in Chinese)

[36] LI Sheng-yi, DAI Yi-fang, PENG Xiao-qiang. Precision modeling for precision and ultra precision machine tools [M]. Changsha: National University of Defense Technology press, 2007: 15−27. (in Chinese)

[37] LIU You-wu. Houston method and its development of multi-body dynamics [J]. China Mechanical Engineering, 2000, 11(6): 601−607. (in Chinese)

[38] FU Guo-qiang, FU Jian-zhong, XU Yue-tong CHEN Zi-chen. Product of exponential model for geometric error integration of multi-axis machine tools [J]. International Journal of Advanced Manufacturing Technology, 2014, 71: 1659−1663.

(Edited by YANG Hua)